

Characterization of $\text{CuIn}_{1-x}\text{Ga}_x\text{Se}_2$ films prepared by spin-coating and co-reduction method

Jing Li, Kegao Liu*, Qilei Sun, Zhigang Wang and Haiyang Wu

School of Materials Science and Engineering, Co-Innovation Center for Green Building of Shandong Province, Shandong Jianzhu University, Fengming Road, Jinan 250101, China

$\text{CuIn}_{1-x}\text{Ga}_x\text{Se}_2$ film has excellent photovoltaic performance due to its large optical absorption coefficient and direct-band gap. It was prepared by spin-coating and chemical co-reduction method which is a simple and easy way with low cost in this work. The surface morphology of the product film was observed using scanning electron microscope (SEM). The absorbance curves are measured by visible spectrophotometer. The phases of the samples were characterized by X-ray diffraction (XRD). It was found by phase analysis that prolonging the reaction time and increasing the reaction temperature were beneficial to the sample crystallization. With the doping concentration increasing, the surface morphology of $\text{CuIn}_{1-x}\text{Ga}_x\text{Se}_2$ films changed with a tendency from spherical crystals to rods. The effect of doping concentration on the resistivity is not particularly obvious. As the doping concentration increases, the resistivity will increase slightly; When $x=1$, the resistivity changes greatly, which may be due to the poor film continuity. Their estimated band gaps of $\text{CuIn}_{1-x}\text{Ga}_x\text{Se}_2$ films are 1.25 eV, 1.3 eV, 1.33 eV, 1.38 eV and 1.4 eV respectively.

Keywords: $\text{CuIn}_{1-x}\text{Ga}_x\text{Se}_2$, morphology, band gap, photovoltaic, solar cell

Introduction

The optimal band gap for a single junction solar cell is about 1.4 eV. Pure CuInSe_2 with a gap 1.04 eV has excellent photoelectric performance [1, 2]. Doping is an important means to regulate the properties of materials [3-5], the enhancement of the thermoelectric properties of the SrTiO_3 by doping with Zr were investigated [6]. To increase the width of CuInSe_2 band gap, indium can be partially replaced by gallium and then it can obtain the compound of copper indium gallium diselenide (CIGSe). CIGSe polycrystalline thin film is recently being developed as an absorber material for thin-film photovoltaic solar cells, it is a multi-crystalline semiconductor of p-type with high-quality characteristics, such as its large optical absorption coefficient and direct-band gap [7]. Light trapping was studied in ultrathin $\text{CuIn}_{1-x}\text{Ga}_x\text{Se}_2$ solar cells by dielectric nanoparticles [8]. CuInSe_2 nanowire arrays with core-shell structure were electrodeposited at various duty cycles into anodic alumina templates [9]. The influence of process parameters were investigated on the gallium composition of a $\text{CuIn}_{1-x}\text{Ga}_x\text{Se}_2$ solar cell [10]. It reported the effects of substrate temperatures in the three-stage growth of $\text{CuIn}_{1-x}\text{Ga}_x\text{Se}_2$ thin films and their photovoltaic performances [11]. The structural and optical properties of Cu-poor $\text{CuIn}_{1-x}\text{Ga}_x\text{Se}_2$ films with different gallium contents prepared by co-evaporated

technique were studied [12]. The effect of growth conditions on the properties of sputtered precursor thin films for $\text{CuIn}_{1-x}\text{Ga}_x\text{Se}_2$ (CIGS) absorber layers was reported [13]. Single phase polycrystalline copper indium gallium diselenide thin-films for solar photovoltaic applications were fabricated by an economical two-stage method of pulsed current electrodeposition [14]. Other research works include simulations about $\text{CuIn}_{1-x}\text{Ga}_x\text{Se}_2$ alloys [15], 3-stage deposition of $\text{CuIn}_{1-x}\text{Ga}_x\text{Se}_2$ on Mo-coated glass and stainless steel substrates [16], $\text{CuIn}_{1-x}\text{Ga}_x\text{Se}_2$ nanopowders or nanoparticles produced by solvothermal method [17, 18] and $\text{CuIn}_{1-x}\text{Ga}_x\text{Se}_2$ prepared by electrodeposition [19]. It has reported our work about CuInSe_2 films prepared from chlorides under different conditions [20]. Quaternary compound $\text{CuIn}_{1-x}\text{Ga}_x\text{Se}_2$ was prepared by spin-coating and chemical co-reduction method in this work.

Experimental

The corresponding amounts of raw materials were weighed according to the stoichiometric ratio of $\text{CuIn}_{1-x}\text{Ga}_x\text{Se}_2$, the precursor solution with the highest concentration was prepared, and the mixture was shaken by the ultrasonic cleaner to make it uniformly mixed. The $\text{CuIn}_{1-x}\text{Ga}_x\text{Se}_2$ precursor film was prepared by spin-coating with 3,000 rpm for 10 seconds, and then the sample was placed in a reaction vessel containing hydrazine hydrate for heat treatment at a certain temperature. Then the $\text{CuIn}_{1-x}\text{Ga}_x\text{Se}_2$ film sample was obtained after soaking in ionized water for 24 h and

*Corresponding author:
Tel : +86-15610183153
E-mail: liukg163@163.com

drying at room temperature. The surface morphology of the product film was observed using scanning electron microscope (SEM). The absorbance curves are measured by Model 723PC visible spectrophotometer made by Shanghai Precision Instrument Co., Ltd. According to the light absorption characteristics of the absorbance curve in the visible light region, the band gap widths of the CuInSe_2 film samples were estimated using extrapolation. The phases of the samples were characterized by X-ray diffraction (XRD).

Preparation and Characterization of $\text{CuIn}_{1-x}\text{Ga}_x\text{Se}_2$ films

$\text{CuIn}_{1-x}\text{Ga}_x\text{Se}_2$ films were prepared by spin-coating and chemical co-reduction method

The phases of $\text{CuIn}_{1-x}\text{Ga}_x\text{Se}_2$ films prepared by different reaction time

Fig. 1 shows the XRD patterns of $\text{CuIn}_{1-x}\text{Ga}_x\text{Se}_2$ obtained with different reaction time of 5 h, 10 h and 20 h at 220 °C. It can be seen that the samples with long reaction time have higher XRD peak intensities, and the reaction time extension is favorable for the crystallization of the film samples. Compared with the standard PDF card with No.89-5649, the XRD patterns of the $\text{CuIn}_{0.9}\text{Ga}_{0.1}\text{Se}_2$ film samples in Fig.1a show three high peaks with 2θ angles at 26.67°, 44.32° and 52.47° that correspond to the (112), (220) and (312) crystal planes respectively; According to the standard PDF card with No.88-2043, the XRD peak of impurity phase Cu_2Se appears in Fig. 1(a), where the 2θ angle 27.12° corresponds to the (111) crystal plane. Fig. 1(b) indicates that the $\text{CuIn}_{0.8}\text{Ga}_{0.2}\text{Se}_2$ film samples reacted with 5 h and 10 h have no XRD peaks corresponding to the target phase while the XRD intensity are very low. The target XRD peaks occur in the sample with the reaction time 20 h; Impurity CuSe appeared in the sample obtained with reaction time 10 h. Fig. 1(c) and (d) show the XRD patterns of $\text{CuIn}_{0.7}\text{Ga}_{0.3}\text{Se}_2$ and $\text{CuIn}_{0.6}\text{Ga}_{0.4}\text{Se}_2$ film samples, compared with the standard PDF card with No.89-5649, the XRD peak positions with 2θ angles are slightly shifted to the right, while the impurity phase Cu_2Se also appeared in the sample reacted for 20 h in Fig. 1(c). It can be seen from Fig. 1(e) that the XRD intensities for the target phase of the $\text{CuIn}_{0.5}\text{Ga}_{0.5}\text{Se}_2$ sample are lower than others and increase with the reaction time prolongation. $\text{CuIn}_{0.4}\text{Ga}_{0.6}\text{Se}_2$ film samples with good crystallinity are obtained under different reaction conditions as shown in Fig. 1(f). It can be seen from Fig. 1(g) that the $\text{CuIn}_{0.3}\text{Ga}_{0.7}\text{Se}_2$ sample with reaction time 5 h has no XRD peaks. As the reaction time increases to 10 h and 20 h, the $\text{CuIn}_{0.3}\text{Ga}_{0.7}\text{Se}_2$ sample crystallizes better and better, but impurity phase Cu_2Se appeared when 20 h. Fig. 1(h) shows that the $\text{CuIn}_{0.2}\text{Ga}_{0.8}\text{Se}_2$ samples did not show the XRD peaks of the target phase with the reaction time 5 h and 10 h, and the XRD peak

appeared when the reaction time extended to 20 h. Compared with the standard PDF card No.89-5649 in Fig. 1(i), the 2θ angle positions of XRD peaks for the $\text{CuIn}_{0.1}\text{Ga}_{0.9}\text{Se}_2$ samples are shifted to the right as a whole. The XRD peaks of the CuGaSe_2 sample correspond to the standard PDF card with No.31-456, and the 2θ angles with 27.7°, 46.11° and 54.25° correspond to (112), (204) and (312) crystal planes of CuGaSe_2 respectively as shown in Fig. 1(j).

Phases of $\text{CuIn}_{1-x}\text{Ga}_x\text{Se}_2$ films prepared at different reaction temperatures

Fig. 2 shows the XRD patterns of $\text{CuIn}_{1-x}\text{Ga}_x\text{Se}_2$ samples reacted at different temperatures for 20 h, compared with the standard PDF card with No.89-5649, the XRD peaks of 2θ angles of 26.67°, 44.32° and 52.47° correspond to (112), (220) and (312) crystal planes respectively. It can be seen from Fig. 2(a) that $\text{CuIn}_{0.9}\text{Ga}_{0.1}\text{Se}_2$ film samples are all with better crystallinity obtained at three temperatures, but impurity phase Cu_2Se also appears, among which $\text{CuIn}_{0.9}\text{Ga}_{0.1}\text{Se}_2$ sample prepared at 200 °C has best crystallinity. Fig. 2(b) indicates that $\text{CuIn}_{0.8}\text{Ga}_{0.2}\text{Se}_2$ film samples have impurity phase Cu_2Se while the sample with best crystallinity was obtained at 220 °C. Fig. 2(c) and Fig. 2(d) show that the XRD peak intensity and sharpness of $\text{CuIn}_{0.7}\text{Ga}_{0.3}\text{Se}_2$ and $\text{CuIn}_{0.6}\text{Ga}_{0.4}\text{Se}_2$ samples prepared at 220 °C are significantly higher than others, but Fig. 2(d) shows a higher XRD peak for impurity phase Cu_2Se . Fig. 2(e) and Fig. 2(f) show that the XRD peak intensities of $\text{CuIn}_{0.5}\text{Ga}_{0.5}\text{Se}_2$ and $\text{CuIn}_{0.4}\text{Ga}_{0.6}\text{Se}_2$ samples prepared at 220 °C are significantly higher than those obtained at 180 °C and 200 °C while impurity phase Cu_2Se appears at 220 °C. Fig. 2(g) shows that the XRD intensity of the $\text{CuIn}_{0.3}\text{Ga}_{0.7}\text{Se}_2$ sample prepared at 180 °C is very low and become greatly high for the sample obtained at 220 °C. Fig. 2(h) shows that there are no obvious XRD peaks for $\text{CuIn}_{0.2}\text{Ga}_{0.8}\text{Se}_2$ sample prepared at 180 °C, which indicates that no target phase appears, when the reaction temperatures were raised to 200 °C and 220 °C respectively, the XRD peaks for target phase appeared, the film sample prepared at 220 °C has higher XRD peak intensity and better crystallinity. Fig.2i shows that $\text{CuIn}_{0.1}\text{Ga}_{0.9}\text{Se}_2$ film sample obtained at 220 °C has higher XRD peak intensity and better crystallinity.

Comparison of XRD patterns of $\text{CuIn}_{1-x}\text{Ga}_x\text{Se}_2$ prepared at 220 °C for 20 h

Fig. 3 shows the XRD patterns of $\text{CuIn}_{1-x}\text{Ga}_x\text{Se}_2$ with doping concentrations of 0.2, 0.4, 0.6 and 0.8 and 1.0 prepared at 220 °C for 20 h. It can be seen that, as the Ga doping concentration increases, the characteristic XRD peaks of the samples gradually shift toward the large diffraction angles. For example, as shown along the (112) crystal plane, the 2θ angle of CuGaSe_2 is about 0.57° larger than that of $\text{CuIn}_{0.8}\text{Ga}_{0.2}\text{Se}_2$.

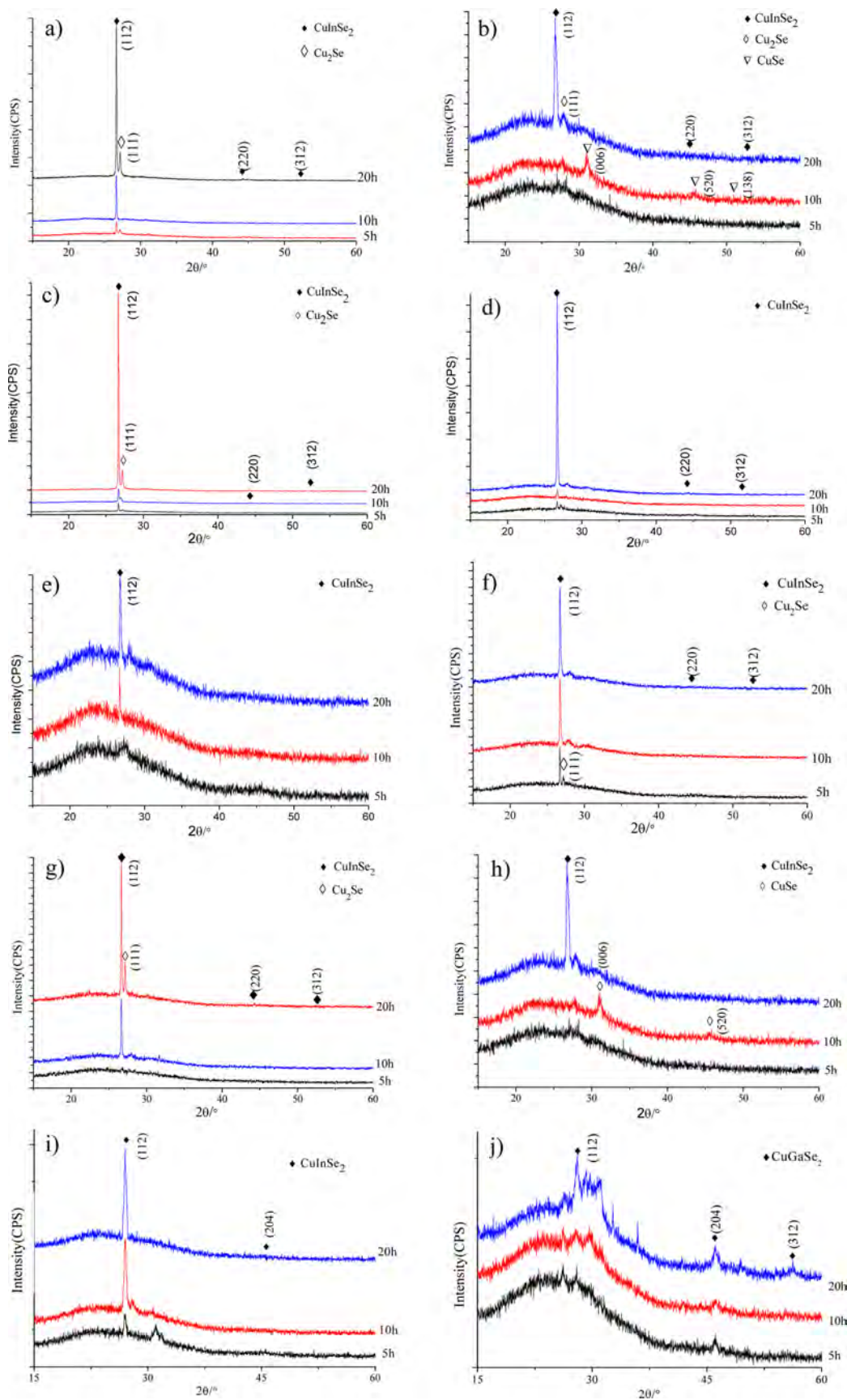


Fig. 1. XRD patterns of $\text{CuIn}_{1-x}\text{Ga}_x\text{Se}_2$ prepared at 220 °C for different reaction time. (a) $\text{CuIn}_{0.9}\text{Ga}_{0.1}\text{Se}_2$, (b) $\text{CuIn}_{0.8}\text{Ga}_{0.2}\text{Se}_2$, (c) $\text{CuIn}_{0.7}\text{Ga}_{0.3}\text{Se}_2$, (d) $\text{CuIn}_{0.6}\text{Ga}_{0.4}\text{Se}_2$, (e) $\text{CuIn}_{0.5}\text{Ga}_{0.5}\text{Se}_2$, (f) $\text{CuIn}_{0.4}\text{Ga}_{0.6}\text{Se}_2$, (j) $\text{CuIn}_{0.3}\text{Ga}_{0.7}\text{Se}_2$, (h) $\text{CuIn}_{0.2}\text{Ga}_{0.8}\text{Se}_2$, (i) $\text{CuIn}_{0.1}\text{Ga}_{0.9}\text{Se}_2$, (j) CuGaSe_2 .

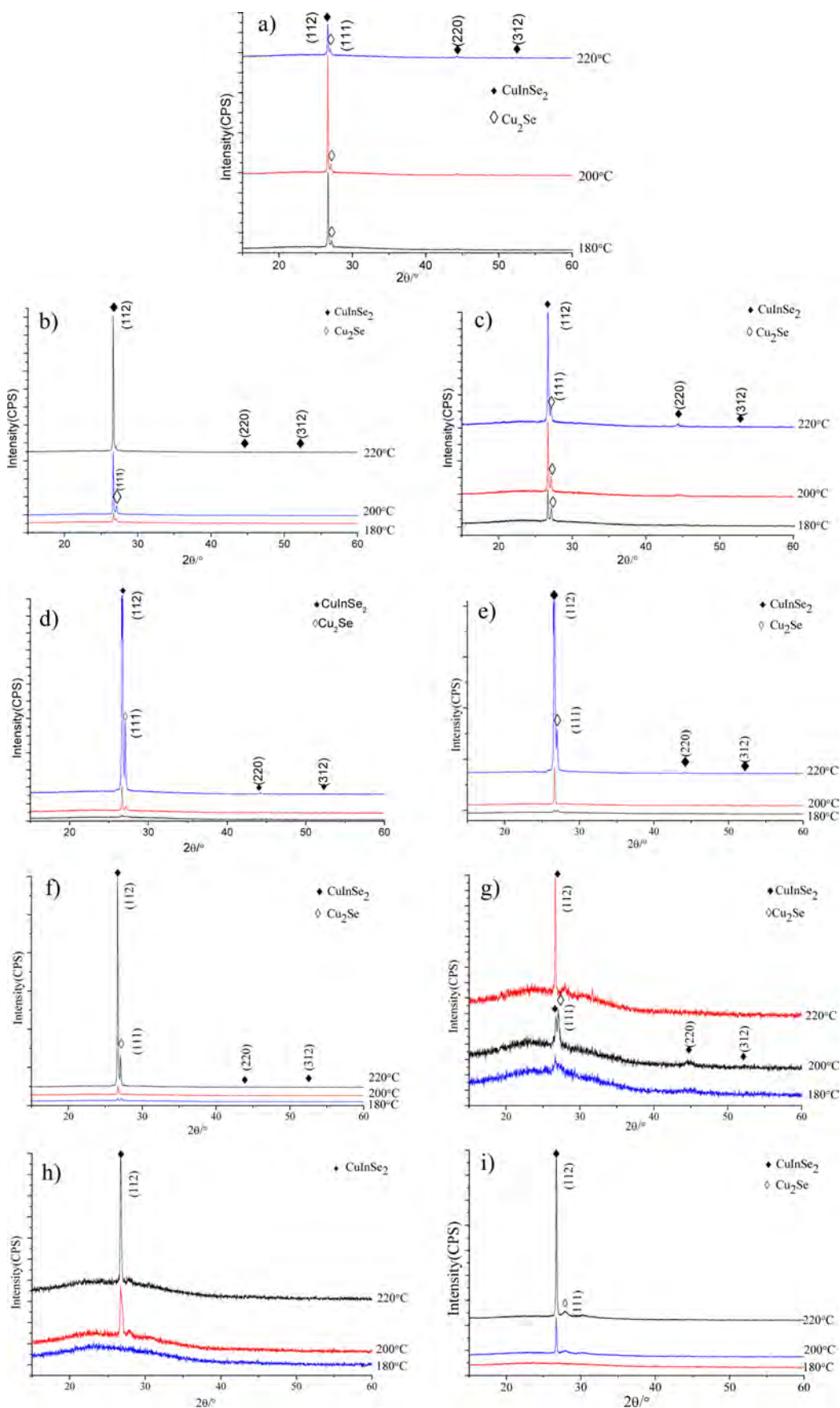


Fig. 2. XRD patterns of $\text{CuIn}_{1-x}\text{Ga}_x\text{Se}_2$ reacted at different temperatures for 20 h. (a) $\text{CuIn}_{0.9}\text{Ga}_{0.1}\text{Se}_2$, (b) $\text{CuIn}_{0.8}\text{Ga}_{0.2}\text{Se}_2$, (c) $\text{CuIn}_{0.7}\text{Ga}_{0.3}\text{Se}_2$, (d) $\text{CuIn}_{0.6}\text{Ga}_{0.4}\text{Se}_2$, (e) $\text{CuIn}_{0.5}\text{Ga}_{0.5}\text{Se}_2$, (f) $\text{CuIn}_{0.4}\text{Ga}_{0.6}\text{Se}_2$, (j) $\text{CuIn}_{0.3}\text{Ga}_{0.7}\text{Se}_2$, (h) $\text{CuIn}_{0.2}\text{Ga}_{0.8}\text{Se}_2$, (i) $\text{CuIn}_{0.1}\text{Ga}_{0.9}\text{Se}_2$.

Analysis of electrical properties of $\text{CuIn}_{1-x}\text{Ga}_x\text{Se}_2$ films

The resistivities of $\text{CuIn}_{1-x}\text{Ga}_x\text{Se}_2$ films are shown in Fig. 4, and the influence of doping concentration on the

resistivity are not obvious. As the doping concentration increases, the resistivity will increase slightly, and when $x=1$, the resistivity changes greatly, it may be due to poor continuity of the film sample.

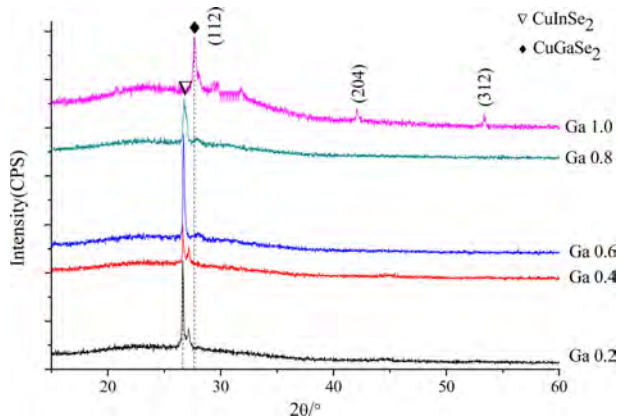


Fig. 3. XRD patterns of $\text{CuIn}_{1-x}\text{Ga}_x\text{Se}_2$ with different doping concentrations prepared at 220 °C for 20 h.

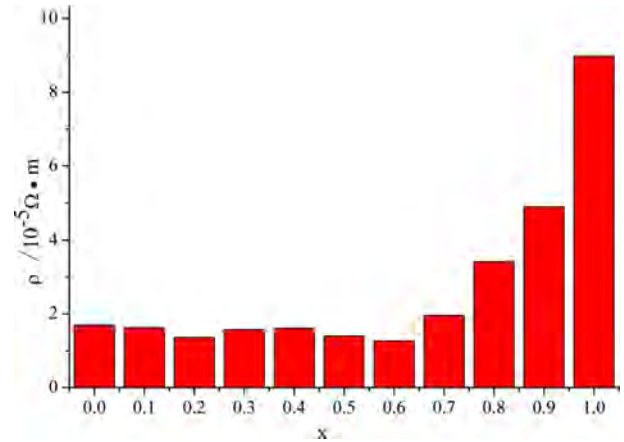


Fig. 4. The resistivities of $\text{CuIn}_{1-x}\text{Ga}_x\text{Se}_2$ films with different doping concentrations prepared at 220 °C for 20 h.

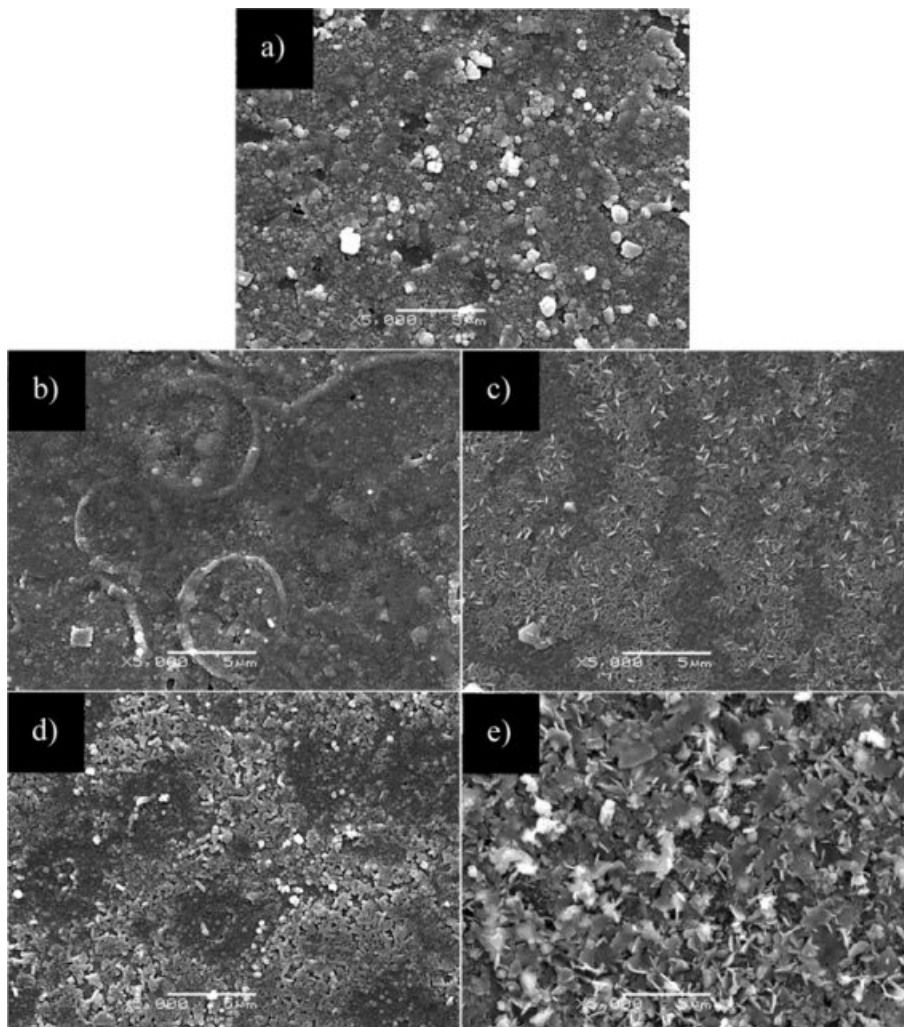


Fig. 5. SEM images of $\text{CuIn}_{1-x}\text{Ga}_x\text{Se}_2$ with different doping concentrations prepared at 220 °C for 20 h. (a) $\text{CuIn}_{0.8}\text{Ga}_{0.2}\text{Se}_2$, (b) $\text{CuIn}_{0.6}\text{Ga}_{0.4}\text{Se}_2$, (c) $\text{CuIn}_{0.4}\text{Ga}_{0.6}\text{Se}_2$, (d) $\text{CuIn}_{0.2}\text{Ga}_{0.8}\text{Se}_2$, (e) CuGaSe_2 .

Morphology analysis of $\text{CuIn}_{1-x}\text{Ga}_x\text{Se}_2$ thin films

Fig. 5 shows the SEM images of $\text{CuIn}_{0.8}\text{Ga}_{0.2}\text{Se}_2$, $\text{CuIn}_{0.6}\text{Ga}_{0.4}\text{Se}_2$, $\text{CuIn}_{0.4}\text{Ga}_{0.6}\text{Se}_2$, $\text{CuIn}_{0.2}\text{Ga}_{0.8}\text{Se}_2$ and CuGaSe_2 film samples prepared at 220°C for 20 h respectively. It can be seen that the $\text{CuIn}_{0.8}\text{Ga}_{0.2}\text{Se}_2$ and $\text{CuIn}_{0.6}\text{Ga}_{0.4}\text{Se}_2$ films are dense and continuous and composed of spherical crystals with diameters of about 0.2 to 0.3 μm , $\text{CuIn}_{0.6}\text{Ga}_{0.4}\text{Se}_2$ film has a non-uniform particle size. The $\text{CuIn}_{0.4}\text{Ga}_{0.6}\text{Se}_2$ film is composed of rod-like crystals with lengths of about 0.8 to 1.0 μm , and its shape is similar to rod shape gathered together with crystal grains. The $\text{CuIn}_{0.2}\text{Ga}_{0.8}\text{Se}_2$ film consists of small rod-like crystals with lengths of about 0.3 to 0.5 μm , and its length and size are smaller than those of the $\text{CuIn}_{0.4}\text{Ga}_{0.6}\text{Se}_2$ film. The CuGaSe_2 film is composed of rod-like crystals with lengths of about 0.8 to 1.0 μm and irregular sheet crystals.

Composition analysis of $\text{CuIn}_{1-x}\text{Ga}_x\text{Se}_2$ film by EDS

Fig. 6 shows the EDS spectrums of $\text{CuIn}_{0.2}\text{Ga}_{0.8}\text{Se}_2$ film and CuGaSe_2 film prepared by spin-coating and co-reduction method. It can be seen from Fig. 6(a) that Cu, Se, In and Ga elements appear from left to right, it confirmed that the above four elements are contained in the product film, although the element ratio is not necessarily stoichiometric. Fig. 6(b) indicates that CuGaSe_2 film sample consists of Cu, Se and Ga elements.

Estimation of the band gaps of $\text{CuIn}_{1-x}\text{Ga}_x\text{Se}_2$ thin films

The absorption spectrums of the film samples were tested using a UV-Vis method on a visible spectrophotometer. Fig. 7 shows the absorbance of $\text{CuIn}_{1-x}\text{Ga}_x\text{Se}_2$ films with different doping concentrations prepared at 220°C for 20 h. The band gaps of the film samples were then estimated by extrapolation as shown in Fig. 8. It can be seen that the estimated band gaps of $\text{CuIn}_{0.8}\text{Ga}_{0.2}\text{Se}_2$, $\text{CuIn}_{0.6}\text{Ga}_{0.4}\text{Se}_2$, $\text{CuIn}_{0.4}\text{Ga}_{0.6}\text{Se}_2$, $\text{CuIn}_{0.2}\text{Ga}_{0.8}\text{Se}_2$ and

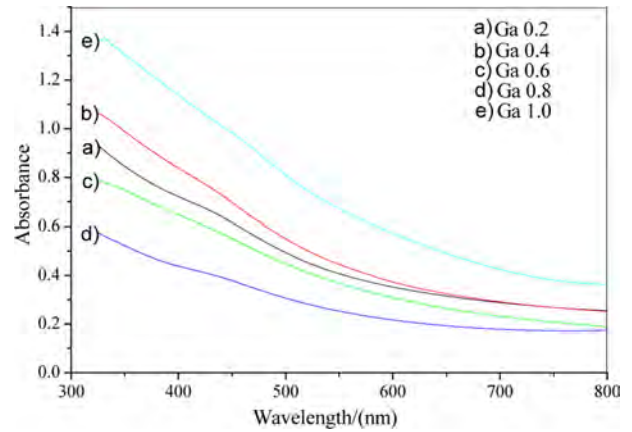


Fig. 7. UV-Vis spectrums of $\text{CuIn}_{1-x}\text{Ga}_x\text{Se}_2$ with different doping concentrations at 220°C for 20 h.

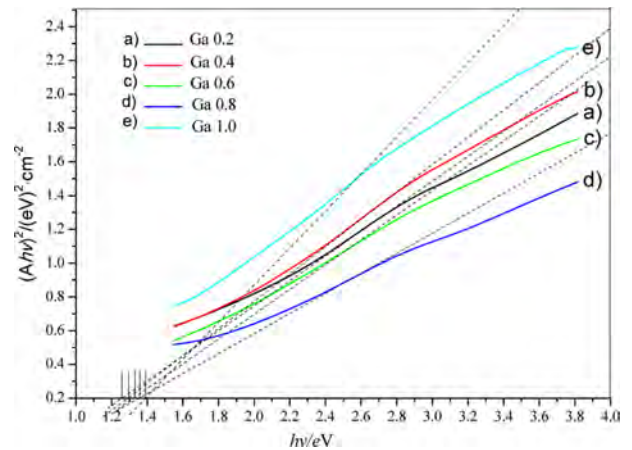


Fig. 8. Estimation of band gaps of $\text{CuIn}_{1-x}\text{Ga}_x\text{Se}_2$ with different doping concentrations at 220°C for 20 h.

CuGaSe_2 films are 1.25 eV, 1.3 eV, 1.33 eV, 1.38 eV and 1.4 eV, respectively.

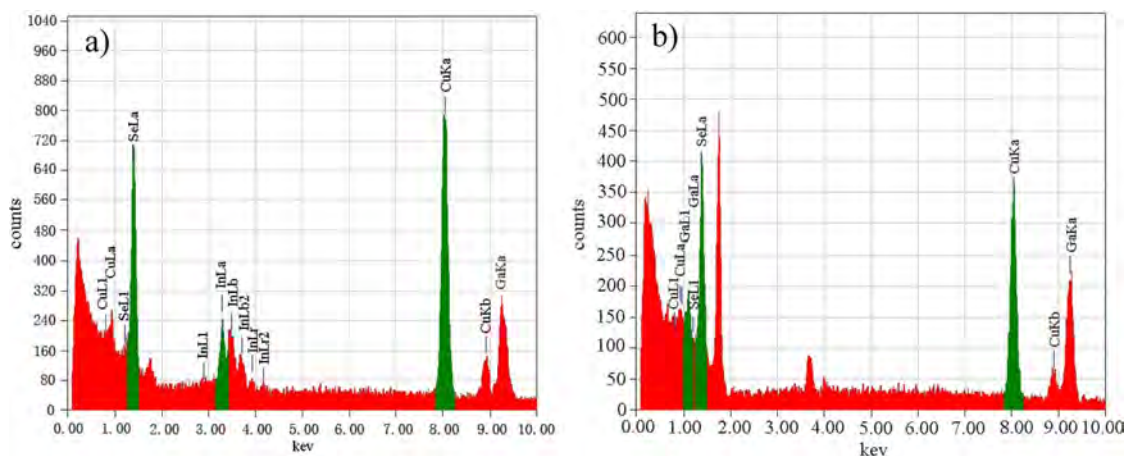


Fig. 6. EDS spectrums of $\text{CuIn}_{0.2}\text{Ga}_{0.8}\text{Se}_2$ and CuGaSe_2 films reacted at 220°C for 20 h. Target products: (a) $\text{CuIn}_{0.2}\text{Ga}_{0.8}\text{Se}_2$, (b) CuGaSe_2 .

Summary

The $\text{CuIn}_{1-x}\text{Ga}_x\text{Se}_2$ films were prepared by spin-coating and co-reduction method. It was found by phase analysis that longer reaction time and higher reaction temperature were beneficial to the sample crystallization, the better experimental conditions for preparing $\text{CuIn}_{1-x}\text{Ga}_x\text{Se}_2$ films are at 220 °C for 20 h. With the increase of doping concentration, the surface morphology of $\text{CuIn}_{1-x}\text{Ga}_x\text{Se}_2$ films changed with a tendency from spherical crystals to rods. The effect of doping concentration on the resistivity is not particularly obvious. As the doping concentration increases, the resistivity will increase slightly. When $x=1$, the resistivity changes greatly, which may be due to the poor continuity of the film. According to the absorbance of $\text{CuIn}_{1-x}\text{Ga}_x\text{Se}_2$ films, their estimated band gaps are 1.25 eV, 1.3 eV, 1.33 eV, 1.38 eV and 1.4 eV, respectively.

Acknowledgement

This work was financially supported by the National Natural Science Foundation of China (No.51272140) and the Innovation Team of the Co-Innovation Center for Green Building of Shandong Province in Shandong Jianzhu University.

References

1. R. Bouferra, G. Marin, S. Amhil, S. M. Wasim, and L. Essaleh, *Physica B*. 565 (2019) 14-17.
2. S.M. Chauhan, S.H. Chaki, M. P. Deshpande, J.P. Tailor, and A.J. Khimani, *Mat. Sci. Semicon. Proc.* 74 (2018) 329-335.
3. Y.J. Park, S.W. Kim, K. Sugimoto, T. Hasegawa, K. Tanima, K. Uematsu, K. Toda, and M. Sato, *J. Ceram. Process. Res.* 20[5] (2019) 460-463.
4. T. Kato, N. Kawaguchi, and T. Yanagida, *J. Ceram. Process. Res.* 20[5] (2019) 449-454.
5. H. Fukushima, D. Nakauchi, N. Kawaguchi, and T. Yanagida, *J. Ceram. Process. Res.* 20[3] (2019) 211-215.
6. T.T. Khan and S.C. Ur, *J. Ceram. Process. Res.* 19[4] (2018) 327-331.
7. A. Aissata and M. Fathib, *J.P. Vilcote, Energy Procedia* 18 (2012) 197-204.
8. G. Yin and P. Manley, *M. Schmid, Sol. Energy* 163 (2018) 443-452.
9. Y.-S. Cheng, N.-F. Wang, Y.-Z. Tsai, J.-J. Lin, and M.-P. Houg, *Appl. Surf. Sci.* 396 (2017) 631-636.
10. C.-S. Chiou and H.-C. Peng, *Sol. Energy* 146 (2017) 436-442.
11. B. Noikaew and S. Chatrathorn, *Surf. Coat. Tech.* 307 (2016) 547-553.
12. Y.-F. Wu, H.-P. Hsu, and H.-I. Chen, *J. Lumin.* 142 (2013) 81-85.
13. M. Behr, M. Sharma, S. Sprague, N. Shinkel, J. Kerbleski, C. Alvey, S. Rozeveld, T. Hasan, C. Wintland, M. Mushrush, and A. Wall, *Thin Solid Films* 665 (2018) 36-45.
14. S. Mandati, B.V.Sarada, S.R. Dey, and S.V. Joshi, *Mater. Lett.* 118 (2014) 158-160.
15. H.T. Xue, F.L. Tang, F.Z. Zhang, W.J. Lu, and Y.D. Feng, *Mater. Lett.* 164 (2016) 169-171.
16. S. Sunkoju, S. Schujman, D. Dixit, A. Diebold, J. Li, R. Collins, and P. Haldar, *Thin Solid Films* 606 (2016) 113-119.
17. A. Khanaki, H. Abdizadeh, and M.R. Golobostanfard, *Mat. Sci. Semicon. Proc.* 16 (2013) 1397-1404.
18. A.B. Marai, J.B. Belgacem, Z.B. Ayadi, K. Djessas, and S. Alaya, *J. Alloy Compd.* 658 (2016) 961-966.
19. R.-W. You, K.K. Lew, and Y.-P. Fu, *Mater. Res. Bull.* 96 (2017) 183-187.
20. K.G. Liu, Y. Xu, Q.L. Sun, H.P. Li, and H.Y. Wu, *Results in Physics*, 12 (2019) 766-770.